Supporting information for

Mechanistic insights into staphylopine-mediated metal acquisition

Liqiang Song*, Yifei Zhang*, Weizhong Chen*, Tongnian Gu*, Shu-Yu Zhang[†], and Quanjiang Ji*[‡]

*School of Physical Science and Technology, ShanghaiTech University, Shanghai 201210, China.

[†]School of Chemistry and Chemical Engineering, Shanghai Jiao Tong University, Shanghai 200240, China.

[‡]To whom correspondence should be addressed:

Quanjiang Ji

School of Physical Science and Technology, ShanghaiTech University

Shanghai 201210, China.

Email: quanjiangji@shanghaitech.edu.cn

Supplementary procedures

Protein expression and purification.

The *cntA* gene was PCR-amplified from *Staphylococcus aureus* Newman genomic DNA with the primers CntA-Fw/Rv (SI Appendix, Table S4). The PCR product was digested with *Nde*I and *Xho*I and further ligated into the *Nde*I/*Xho*I sites of a pET28a-modified vector containing the human rhinovirus 3C (HRV3C) protease cleavage site. The successful construction of the plasmid pET28a_HRV3C_CntA was confirmed by sequencing. The plasmid was transformed into *E.coli* BL21 (DE3) for protein expression. Cells were grown in LB to an OD_{600} of ~0.6 at 37 ℃. Protein expression was induced by adding 0.5 mM IPTG to the growth media. The induced cells were further cultured overnight at 20 ℃. The cells were harvested by centrifugation at 5000 g for 10 min.

Cell pellets were resuspended in the lysis buffer (10 mM Tris·HCl pH 7.4, 500 mM NaCl, 5% glycerol, 1mM DTT), and lysed by sonication. The 6XHis-tagged protein was trapped in a His-Trap HP column (GE Healthcare). The column was first washed with 20 mL lysis buffer and then eluted with a buffer containing 10 mM Tris·HCl pH 7.4, 500 mM NaCl, 5% glycerol, 100 mM imidazole, and 1mM DTT. The protein was buffer exchanged into the lysis buffer using a spin column (molecular-weight cutoff of 10 kDa, Merck Millipore). The 6XHis tag of the protein was cleaved by the HRV 3C protease (the mass ratio of CntA and HRV 3C protease is ~ 100:1) at 4 ^{o}C overnight. The protein was clarified and passed through a His-trap column to remove uncleaved CntA and the HRV 3C protease. The flow-through fraction was collected and further purified by using a HiLoad 16/600 Superdex 200 pg column (GE Healthcare) in the elution buffer (10 mM Tris·HCl pH 7.4, 100 mM NaCl). The eluted protein was concentrated to a

concentration of ~20 mg/mL (the concentration was determined by UV-Vis spectrometry; The extinction coefficient of CntA at 280 nm is ~ 57300 M^{-1} cm^{-1}).

For site-specific mutagenesis of *cntA*, rolling-circle PCR (using the primers listed in Table S4) was performed by following the standard procedures of the QuickChange Site-Directed Mutagenesis Kit (Stratagene). The successful construction of the mutated plasmids was confirmed by sequencing. The mutant proteins were purified by using the same procedures as that of the wild-type protein.

Size-exclusion chromatography.

The CntA wild-type and mutant proteins (after 6XHis tag cleavage) were subjected to size-exclusion chromatography analysis by using a HiLoad 16/600 Superdex 200 pg column (GE Healthcare) in the elution buffer (10 mM Tris·HCl pH 7.4, 100 mM NaCl) at a flow rate of 1 mL/min with UV detection at 280 nm.

Protein crystallization.

The first truncation of CntA we tried to crystallize is from Q35 to K532 (the amino acids are not renumbered). The design of the construct is based on protein sequence alignment with structure-solved solute-binding proteins. However, we could not obtain any crystal after screening 500 conditions. We then performed a protein secondary structure analysis. We noticed that the CntA protein possesses an additional N-terminal helix (G26-N33 [the amino acids are not renumbered]) compared with structure-solved SBPs. We suspected that this helix may affect protein crystallization. After adding the N-terminal helix, the CntA protein was crystallized

successfully. The truncated region before the N-terminal helix is the lipophilic anchor.

The apo-CntA protein and CntA/StP/metal (Co^{2+}, Ni^{2+}, and Zn^{2+}) complexes were crystallized by using the sitting-drop, vapor-diffusion method at 16 °C. To obtain apo-CntA crystals, 1 μL protein solution (15 mg/ml in 10 mM Tris-HCl pH 7.4, 100 mM NaCl) was mixed with an equal volume of reservoir solution containing 0.1 M MES monohydrate pH 5.5, 25% (v/v) polyethylene glycol 400. For co-crystallization, CntA was incubated with metal-bound StP (the molar ratio of CntA and StP/ Ni^{2+} is ~ 1:3) before being mixed with the reservoir solution containing 0.1 M citric acid pH 3.5, 14% (w/v) polyethylene glycol 1000. The CntA/StP/Co^{2+} and CntA/StP/Zn^{2+} complexes were crystallized under the condition containing 0.1 M BICINE pH 8.5, 8% w/v polyethylene glycol monomethyl ether 5000. The crystals were cryo-protected and stored in liquid N_2 before data collection.

Data collection, structure determination, and refinement.

The data were collected at BL18U1 and BL19U1 beamlines of National Facility for Protein Science Shanghai (NFPS) at Shanghai Synchrotron Radiation Facility. The data were processed by HKL3000 (1). The phase of apo-CntA was determined by Phaser (2) from ccp4i (3) suits using the structure of *Brucella suis* NikA (PDB code: 4OER) as the searching model. The phases of the CntA/StP/metal complexes were determined by Phaser using the structure of apo-CntA as the searching model. The models were built by Autobuild from PHENIX (4) suits. The model of CntA/StP/Co^{2+} was refined using phenix.refine from PHENIX (4) suits and the models of apo-CntA, CntA/StP/Ni^{2+} and CntA/StP/Zn^{2+} were refined using Refmac5 from ccp4i suits (using

TLS and restrained refinement for the model of apo-CntA). The models were further improved manually by coot (5). The final structures were visualized by Pymol (http://www.pymol.org).

Isothermal titration calorimetry (ITC).

Staphylopine (N-[3-(N-L-Alanyl)-amino-3-carboxypropyl]-D-histidine) and nicotianamine were ordered from Toronto Research Chemical Inc (Toronto, Canada). The binding constants were determined by using the MicroCal ITC200 system (Malvern). The wild-type CntA protein, the mutant proteins, and the ligands were prepared in the same buffer containing 10 mM Tris-HCl, pH 7.4, 100 mM NaCl. The concentrations of the proteins and the ligands for the assay were 20 μM and 200 μM, respectively. In the assay, the solutions of ligands in the syringe were slowly titrated into the reaction cell containing protein solutions. The assay was performed at 25 ℃ with a stirring speed of 750 rpm. The ligands were injected 20 times (0.4 μl for injection 1 and 2 μl for injections 2–20), with 180 s intervals between injections. The data were analyzed with the Origin7 software package (Malvern).

Construction of *cntA* gene deletion and single-base substitution mutants of *S. aureus*.

The *cntA* gene deletion and single-base substitution mutants were constructed by using the pCasSA system(6).

In brief, a 20-bp spacer sequence (before NGG PAM site), adjacent to the desired mutation site, was cloned into the pCasSA plasmid by Golden Gate assembly. When the desired mutation site is not present in the PAM sequence, a silent mutation was introduced in the PAM to prevent the cutting of Cas9/sgRNA complex in the genome of edited cells. To achieve this, we prepared the

repair arms by using a helper vector pSP72. A ~ 4 kb DNA sequence containing the entire *cntA* gene and the up and down regions of *cntA* was PCR amplified from the Newman genomic DNA. The desired mutation and the silent mutation (when necessary) were introduced into the repair arms by site-directed mutagenesis. The repair template containing the desired mutation and the silent mutation (when necessary) was PCR amplified from the pSP72_cnt plasmid and subsequently cloned into the pCasSA_spacer plasmid by Gibson assembly. The plasmid was first transformed into the RN4220 strain by electroporation. The successful editing in the RN4220 strain was confirmed by sequencing. The plasmid was then isolated from the RN4220 strain that contained the desired mutation and transformed into the Newman strain by electroporation. The successful editing in the Newman strain was confirmed by sequencing. The *cntA* gene deletion mutants were obtained from the literature (6).

cntA gene complementation.

The *cntA* gene and the cnt operon promoter were PCR amplified (Table S4) from the Newman genomic DNA. The PCR products were inserted into the *Bam*HI site of the chromosomal integration vector pCL55 (7) by Gibson assembly to generate the pCL_*cntA* plasmid (the expression of *cntA* is driven by the cnt operon promoter). The pCL_*cntA* plasmid and the empty pCL55 plasmid were first transformed into the *E. coli* ALC7885 (8) strain for restriction modification. The plasmids isolated from the ALC7885 strain were directly transformed into the *S. aureus* Newman strain by electroporation.

Growth curve measurements.

Previous studies (9, 10) revealed that the phenotypes after StP-biosynthesis pathway disruption is most significant when cobalt was utilized for the experiments (growth curve and metal-content measurements). To better assess the role of each StP/metal-binding residues, we utilized cobalt for the experiments. The growth of *S. aureus* strains was monitored using the automated microbe growth curve analysis system BioScreen C (OY Growth Curves Ltd, Finland). Overnight cultures were 1:100 diluted into 200 μL CDM (When indicated, the cultures were supplemented with 1.5 mM $CoCl_2$) and then transferred to the Bioscreen micro-well plates. The plates were incubated at 37 ℃ with continuous shaking inside the machine. The optical density (OD) at 600 nm was measured every 30 min. All the experiments were performed in triplicate.

Metal-content measurement using ICP-AES.

The samples were prepared according to procedures described in the literatures (9, 10). In brief, 10 ml cultures of *S. aureus* strains were grown at 37 ℃ in CDM (supplemented with 1μM $CoCl_2$) until late exponential phase (OD_{600} ~ 1.5-2.5). Cultures were harvested by centrifugation at 6,000 g at 4℃ for 10 min. Pellets were washed three times with 1 mL 1 mM EDTA solution (ice-cold) followed by a wash with 1mL MilliQ H_2O. Cells were dried overnight at 100 ℃ and then digested by 500 μL nitric acid (Suprapur 66~68 % HNO_3; Sinopharm Chemical Reagent Co., Ltd) for 12 hr at 80 ℃. The samples were diluted by adding MilliQ H_2O to final volumes of 5 mL. The element measurements were performed with Inductively Coupled Plasma-Absorption Emission Spectrometer (iCAP 7000 Plus Series, Thermo Scientific™). Concentrations were determined by using standard solutions. The concentration of each metal element was calculated assuming 4 X 10^8 cfu for an OD_{600} of 1 unit. The experiments were performed in triplicate.

Competitive binding assay and metal analysis

StP was incubated with a metal cocktail (Co^{2+}, Ni^{2+}, and Zn^{2+}) for 10 minutes before being added into the 6XHis-tag cleaved CntA protein solution. The reaction was performed in the 1 mL buffer containing 10 mM Tris·HCl, pH 7.5. 560 nmol of StP, 140 nmol of each metal (Co^{2+}, Ni^{2+}, and Zn^{2+}), and 70 nmol of CntA were used in the reaction. Unbounded StP/metal was removed by using a desalting separation (HiTrap column, GE Healthcare). The eluted CntA/StP/metal complexes were collected and lyophilized overnight. The powders were digested by 500 μL nitric acid (Suprapur 66~68 % HNO_3; Sinopharm Chemical Reagent Co., Ltd) for 24 hr at 60 ℃. The samples were diluted by adding MilliQ H_2O to final volumes of 6 mL prior to metal-content determination by ICP-AES. The experiments were performed in triplicate.

Table S1. Data collection, phasing, and refinement statistics.

	CntA (apo form) (5YH5)	CntA/Staphylopine/ Ni^{2+} (5YH8)	CntA/Staphylopine/ Co^{2+} (5YHE)	CntA/Staphylopine/ Zn^{2+} (5YHG)
Wavelength (Å)	0.9778	0.9785	0.9778	0.9778
Beamline[a]	BL18U1	BL19U1	BL18U1	BL18U1
Space group	$P6_1$	$P22_12_1$	P1	$P2_12_12$
Cell dimensions				
a, b, c (Å)	149.395, 149.395, 53.635	70.782, 85.474, 86.315	42.605, 76.659, 85.673	86.07, 156.349, 42.257
α, β, γ (°)	90.00, 90.00, 120.00	90.00, 90.00, 90.00	90.683, 91.251, 104.568	90.00, 90.00, 90.00
Resolution (Å)	50.00-2.90	50.00-2.12	50.00-2.47	50.00-2.03
R_{merge} (%)	23.2 (177.7)[b]	14.1(83.8)	9.6 (43.9)	9.3 (48.8)
I/σI	16.7 (2.0)	16.1 (2.0)	11.1 (2.0)	24.9 (2.3)
Completeness (%)	100.0 (100.0)	99.9 (99.9)	98.0 (97.4)	99.7 (96.8)
Redundancy	20.1 (19.9)	12.7(9.8)	3.5 (3.6)	12.1(9.8)
Refinement				
Resolution (Å)	49.55-2.90	42.74-2.12	36.78-2.47	44.58-2.03
Reflections (#)	15367	30251	37030	37675
R_{work}/R_{free} (%)	19.8/26.8	15.6/22.9	16.1/23.5	15.9/21.3
Number of nonhydrogen Atoms (#)				
Protein	4008	4064	8069	4039
Staphylopine/metal	/	24	48	24
Rmsds				
Bond lengths (Å)	0.017	0.015	0.008	0.018
Bond angle (°)	2.01	1.82	1.00	1.91
Average B factors ($Å^2$)				
Overall	86.94	35.20	38.99	45.50
Protein	86.94	34.60	39.07	45.04
Staphylopine/metal	/	22.68	29.87	37.42

[a]Crystal data were collected at the beamlines of National Facility for Protein Science Shanghai (NFPS) at Shanghai Synchrotron Radiation Facility.

[b]Statistics for the highest-resolution shell are shown in parentheses.

Fig. S1. Sequence alignment of CntA, *Ec*NikA, *Cj*NikZ, and *Bs*NikA. The structural alignment was performed by ESPript online software (http://espript.ibcp.fr/ESPript/cgi-bin/ESPript.cgi). The StP/metal-recognition residues were indicated.

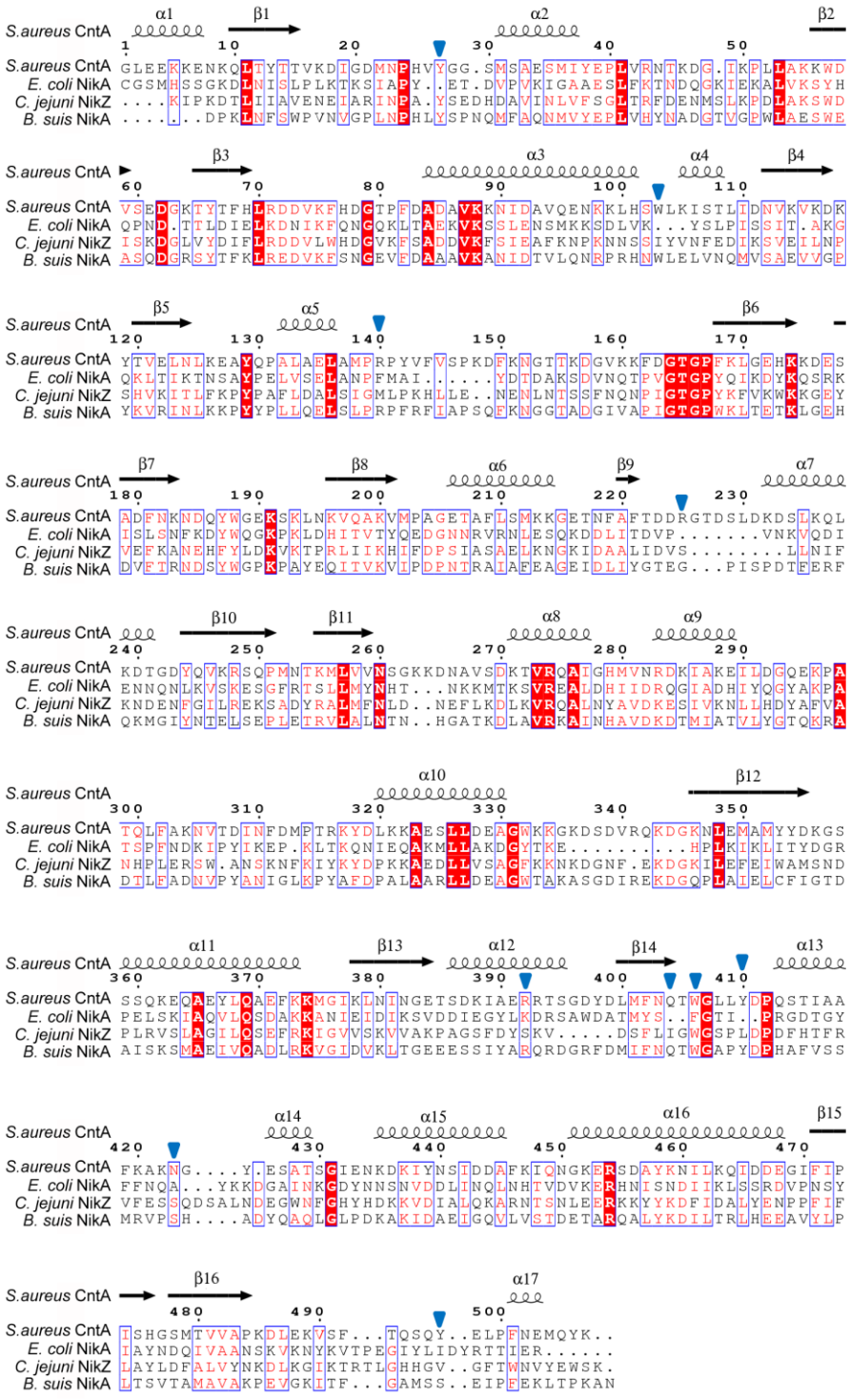

Fig. S2. Schematic representation of the topology of apo-CntA. The assignment of the secondary structure was based on the tertiary structure of apo-CntA visualized by Pymol.

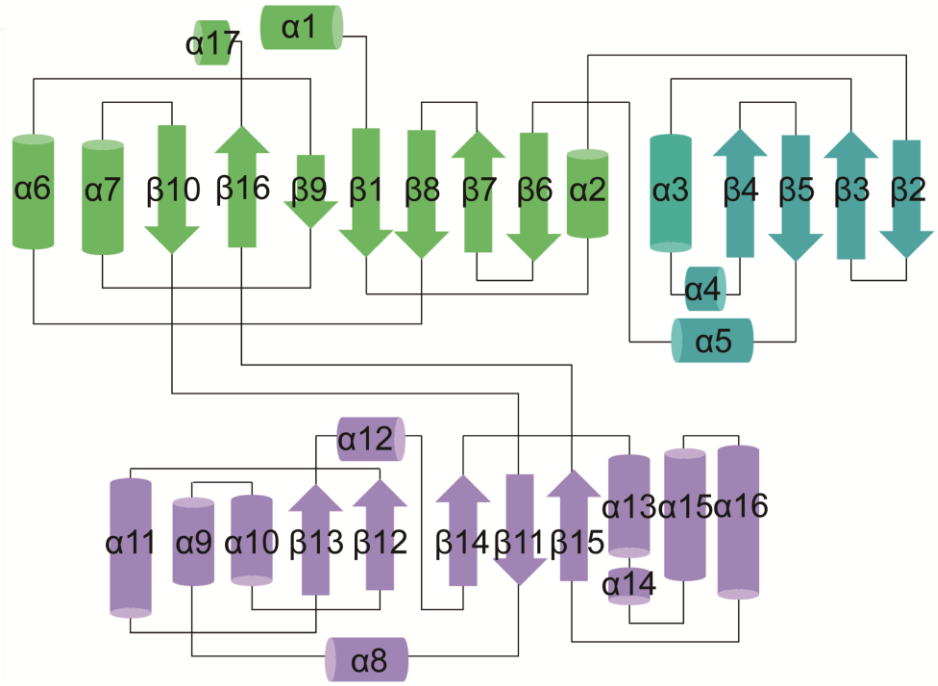

Fig. S3. Both StP and metals are indispensable for CntA binding. (*A*) ITC assay for the binding between CntA and StP/Ni^{2+}. K_d: the dissociation constant; N: the number of binding sites per CntA. (*B*) ITC assay for the binding between CntA and StP/Zn^{2+}. K_d: the dissociation constant; N: the number of binding sites per CntA. (*C*) ITC assay for the binding between CntA and StP. (*D*) ITC assays for the binding between CntA and different metals.

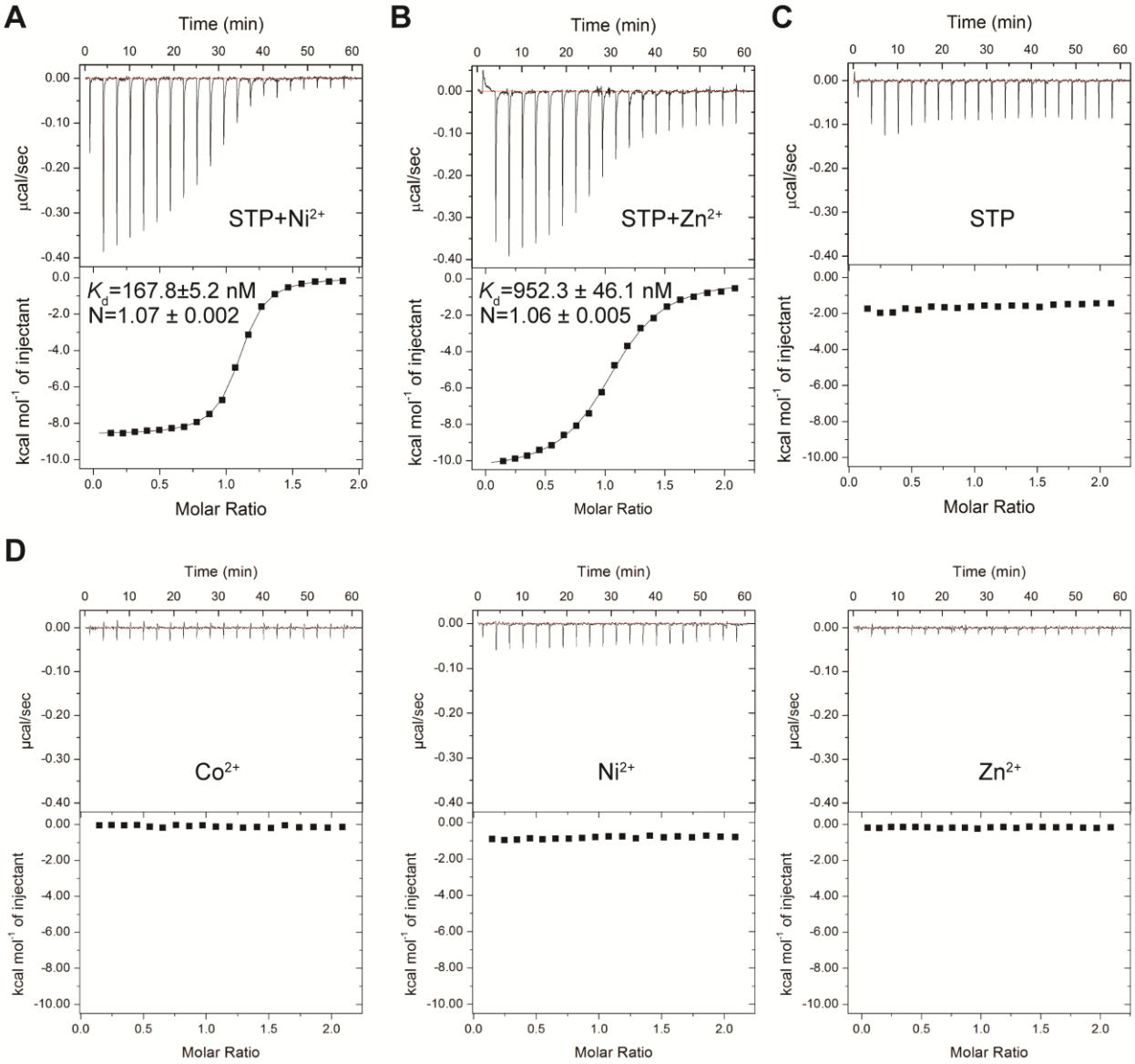

Fig. S4. A competitive binding assay indicates CntA binds StP/Ni^{2+} and StP/Co^{2+} tighter than StP/Zn^{2+}. The assay was performed by incubating 70 μM CntA with 560 μM StP and a metal mixture containing 140 μM Zn^{2+}, 140 μM Ni^{2+}, and 140 μM Co^{2+}. Unbounded StP/metal was removed by desalting. The metal content in CntA was determined by ICP-AES. The experiment was performed in triplicate.

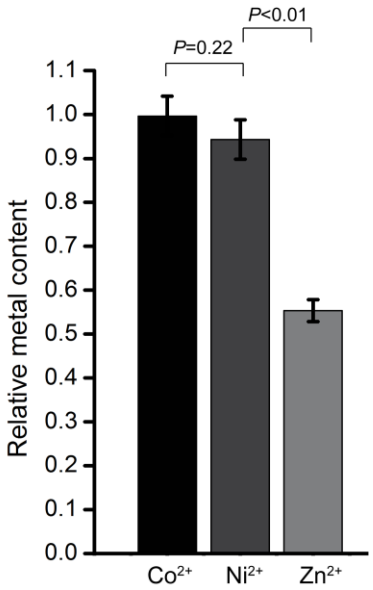

Fig. S5. Structural characterizations of the CntA/StP/Ni^{2+} complex and the CntA/StP/Zn^{2+} complex. (*A*) The overall structure of the CntA/StP/Ni^{2+} complex. StP is colored yellow. (*B*) The surface structure of the CntA/StP/Ni^{2+} complex. (*C*) The overall structure of the CntA/StP/Zn^{2+} complex. StP is colored yellow. (*D*) The surface structure of the CntA/StP/Zn^{2+} complex.

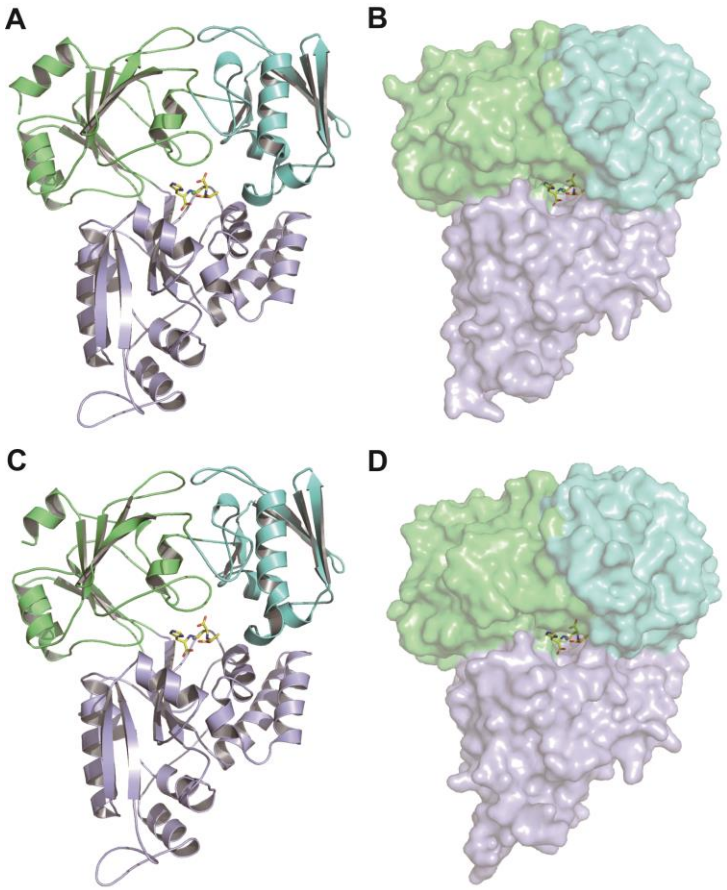

Fig. S6. Electron density maps of StP/Co^{2+}, StP/Ni^{2+}, and StP/Zn^{2+}. (*A*) Detailed view of the electron density of Co^{2+}. $2F_o$-F_c map (6.0 σ) is shown as a blue mesh. (*B*) Detailed view of the electron density of StP/Ni^{2+}. $2F_o$-F_c map (1.0 σ) of StP/Ni^{2+} and $2F_o$-F_c map (6.0 σ) of Ni^{2+} are shown as blue meshes. (*C*) Detailed view of the electron density of StP/Zn^{2+}. $2F_o$-F_c map (1.0 σ) of StP/Zn^{2+} and $2F_o$-F_c map (6.0 σ) of Zn^{2+} are shown as a blue mesh.

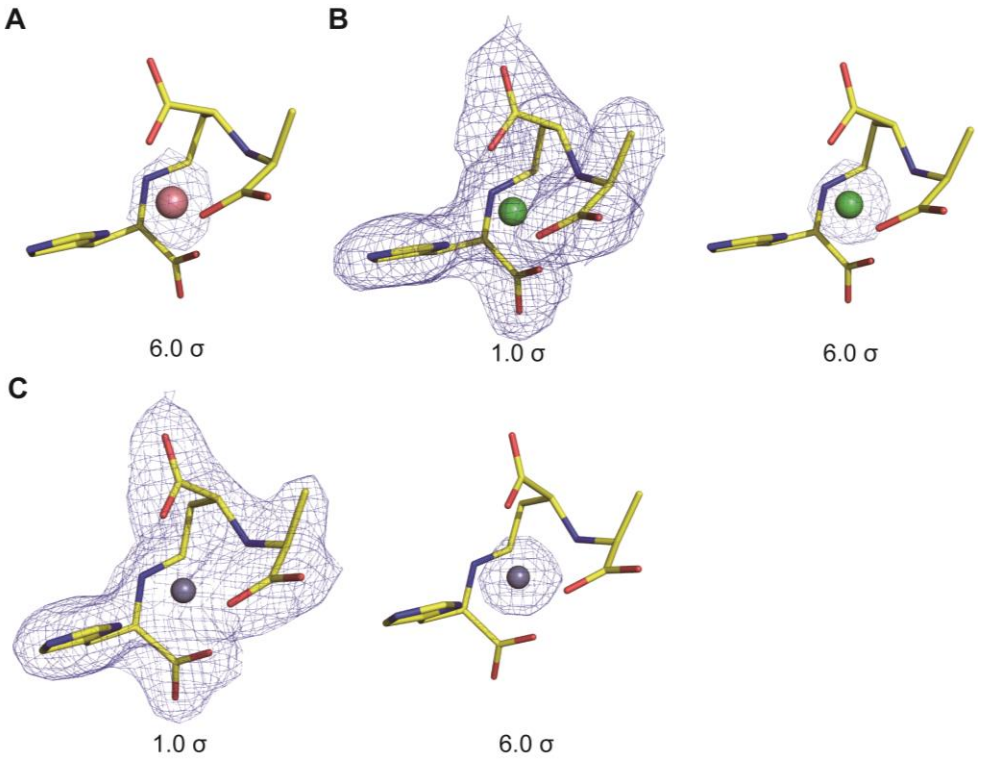

Fig. S7. The structures of three CntA/StP/metal complexes exhibit almost identical overall conformation. (*A*) Structural comparison of the CntA/StP/Co^{2+} complex and the CntA/StP/Ni^{2+} complex by superimposing Cα atoms in overall molecule. The proteins of the CntA/StP/Co^{2+} complex and the CntA/StP/Ni^{2+} complex are colored gray and green, respectively. (*B*) Structural comparison of the CntA/StP/Co^{2+} complex and the CntA/StP/Zn^{2+} complex by superimposing Cα atoms in overall molecule. The proteins of the CntA/StP/Co^{2+} complex and the CntA/StP/Zn^{2+} complex are colored gray and cyan, respectively.

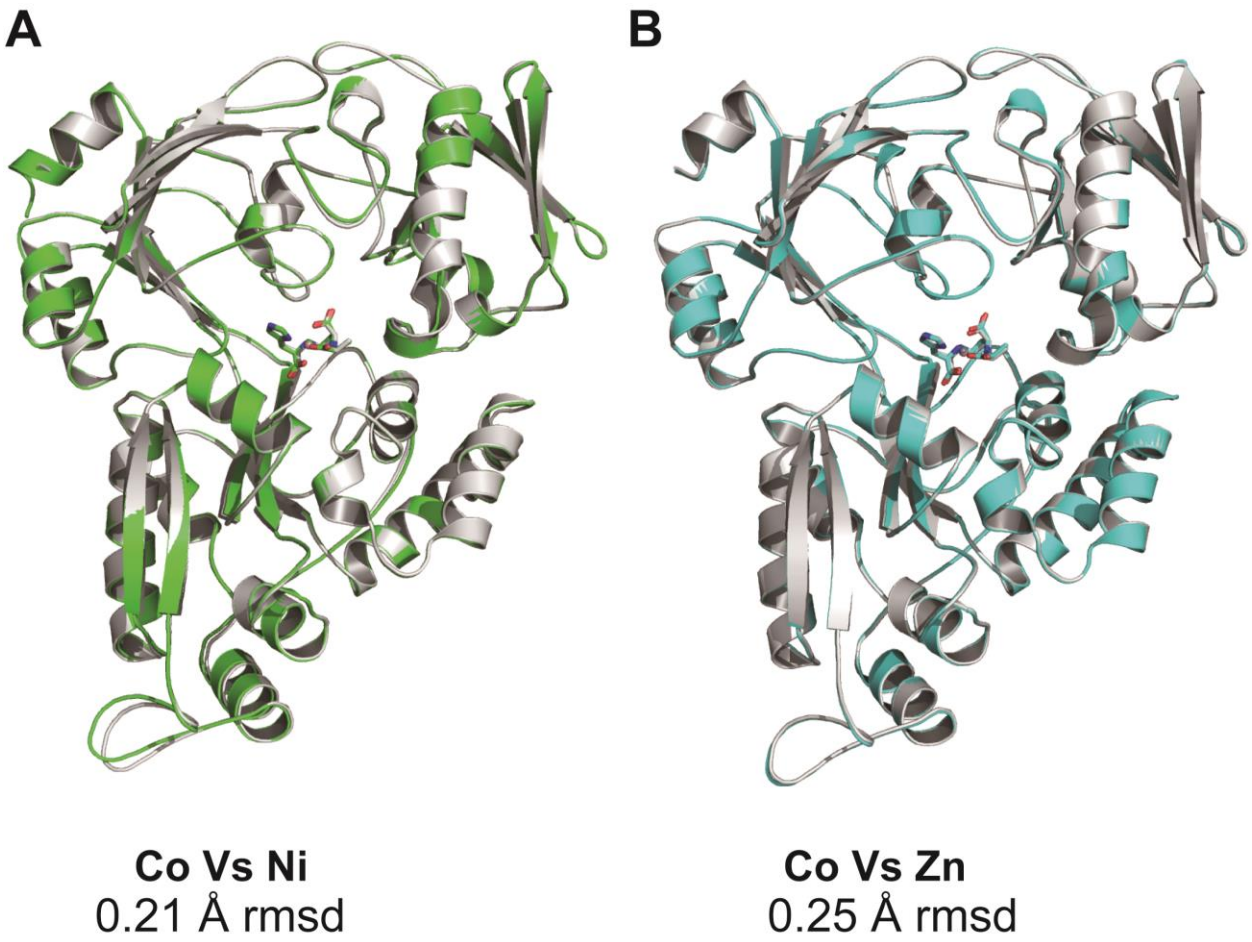

Fig. S8. The binding between CntA and StP/metal is specific and selective. (*A*) ITC assay between CntA and EDTA/Co^{2+}. (*B*) ITC assay between CntA and nicotianamine/Co^{2+}.

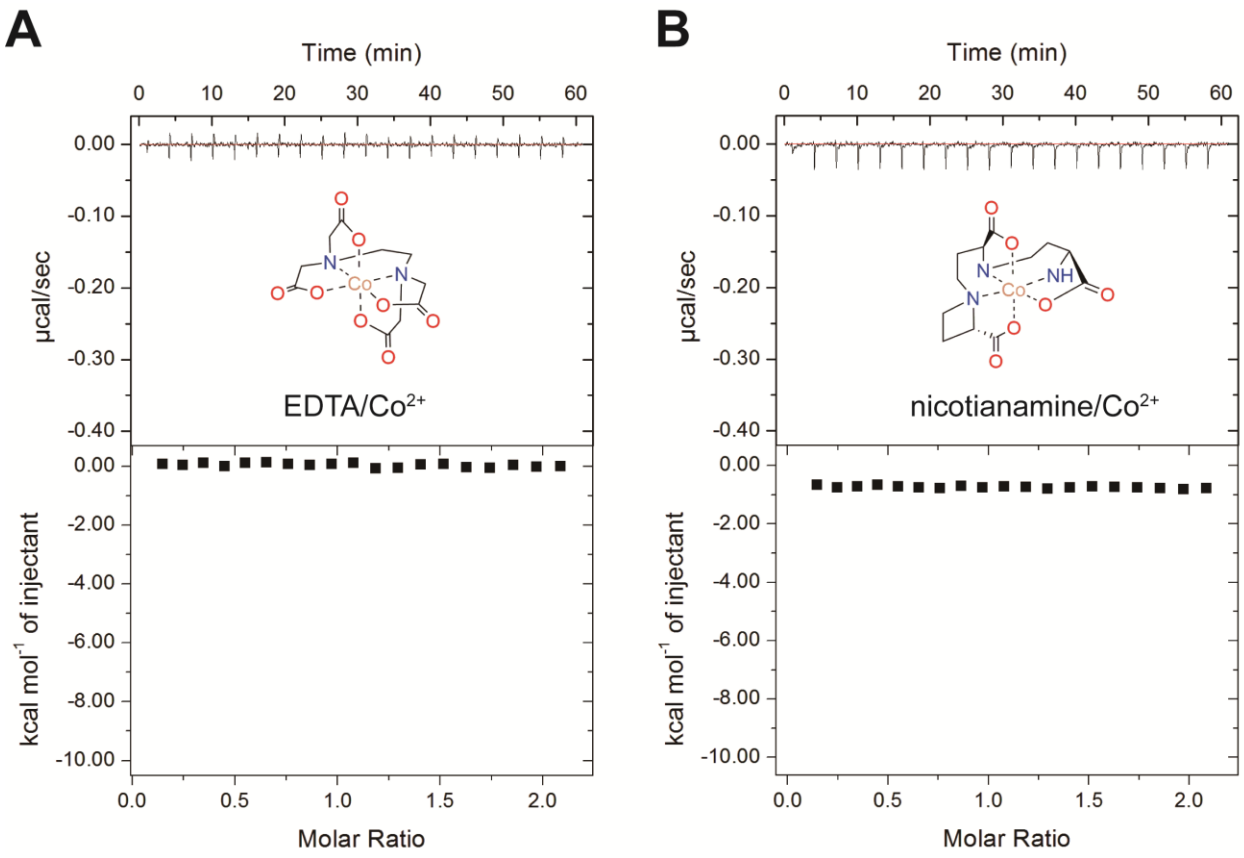

Fig. S9. Structural comparison of the CntA/StP/Co^{2+} complex and apo-CntA by superimposing Cα atoms in domains I_a and I_b. The domain II is viewed as cartoon and the domains I_a and I_b are viewed as ribbon. CntA/StP/Co^{2+} and apo-CntA are colored cyan and salmon, respectively.

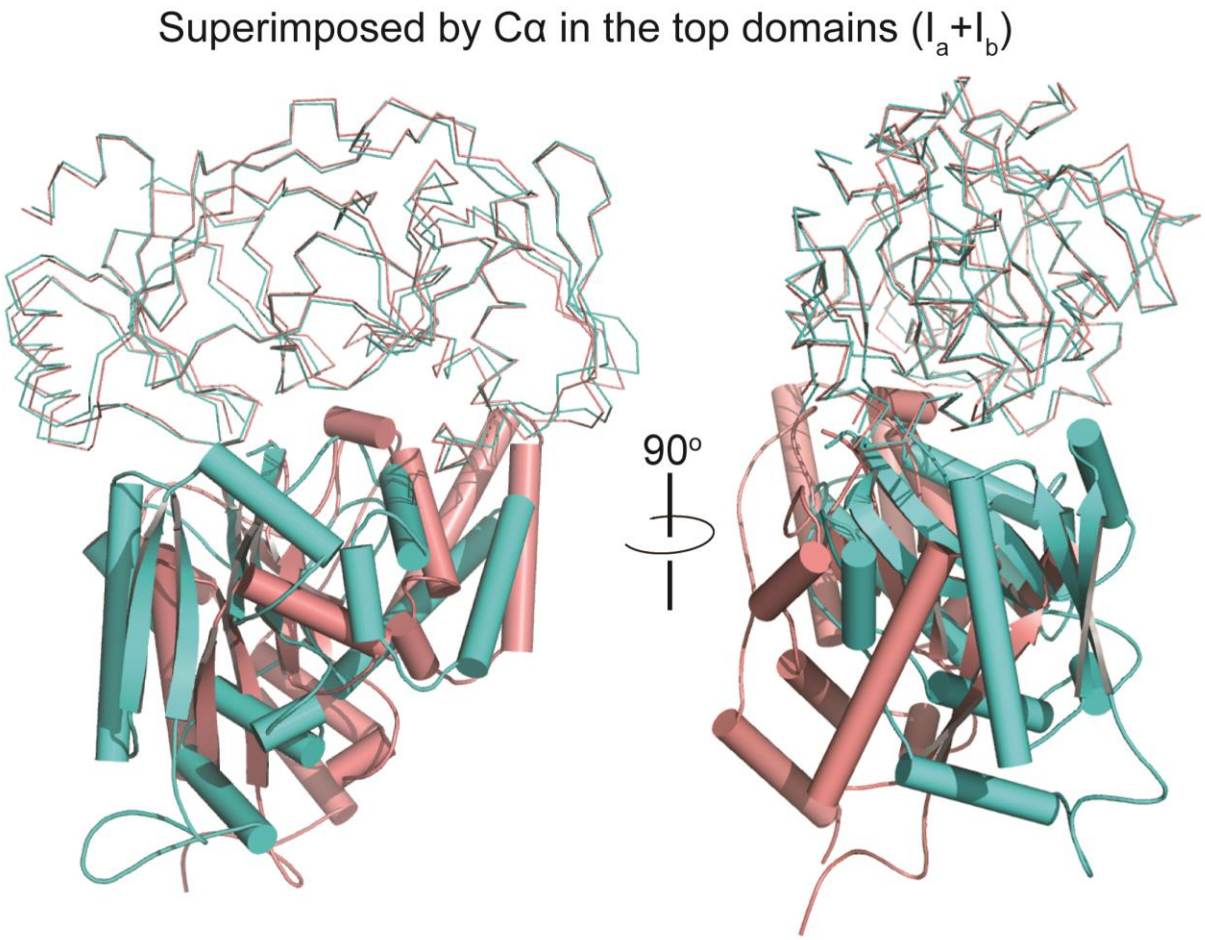

Fig. S10. Ligand binding induces inter-domain conformational change in metal-transportation SBPs. (*A*) Structural comparison between the apo structure of *Brucella suis* NikA (PDB: 4OER) and the *Bs*NikA/EDTA/Fe complex (PDB: 4OES). The apo and the complex structures are colored salmon and cyan, respectively. (*B*) Structural comparison between the apo structure of *Yersinia pestis* YntA (PDB: 4OFO) and the *Yp*YntA/L-histidine/Ni complex (PDB: 4OFL). The apo and the complex structures are colored salmon and cyan, respectively. The black arrows represent the directions that each domain moves.

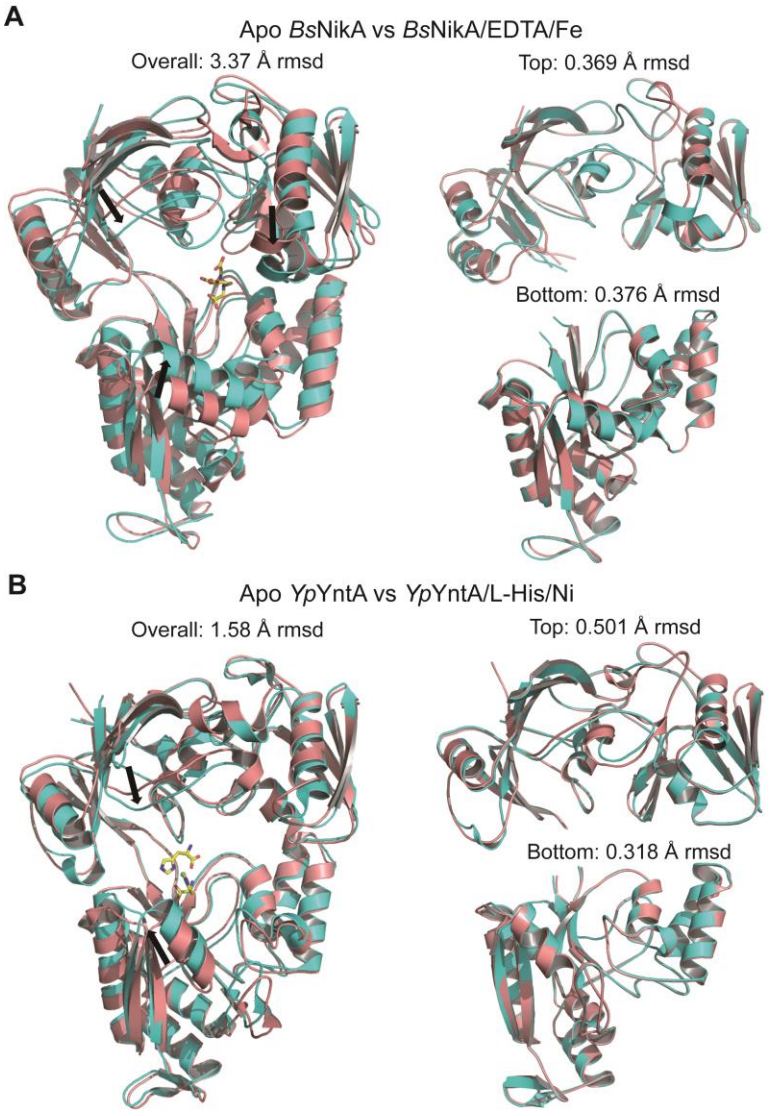

Fig. S11. Ligand binding induces inter-domain conformational change in oligopeptide-transportation SBPs. (*A*) Structural comparison between the apo structure of *Lactococcus lactis* OppA (PDB: 3FTO) and the *Ll*OppA/SLSQLSSQS complex (PDB: 3RYA). The apo and the complex structures are colored salmon and cyan, respectively. (*B*) Structural comparison between the apo structure of *Salmonella typhimurium* OppA (PDB: 1RKM) and the *St*OppA/KK complex (PDB: 2RKM). The apo and the complex structures are colored salmon and cyan, respectively. The black arrows represent the directions that each domain moves.

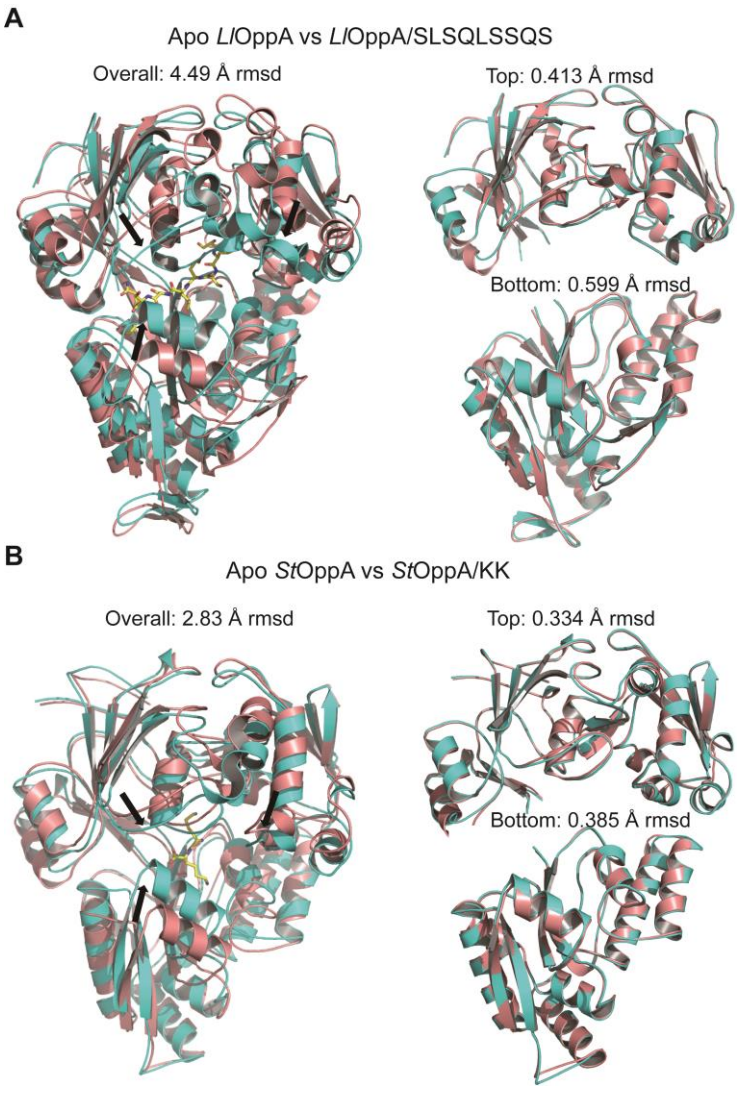

Fig. S12. Cd^{2+} binding induces inter-domain conformational change in *Streptococcus pneumoniae* PsaA. The apo (PDB: 3ZK7) and complex (PDB: 4UTP) structures are colored salmon and cyan, respectively.

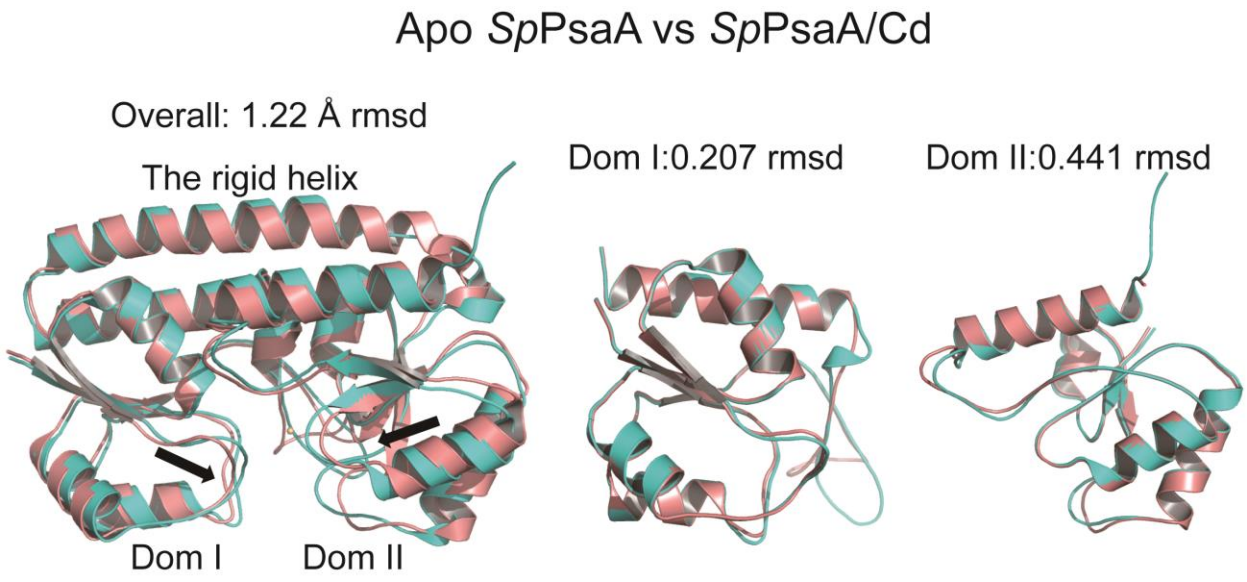

Fig. S13. CntA possesses a unique ligand-recognition mode. (*A*) Superimposition of the structure of CntA/StP/Co^{2+} with that of *Sa*NikA/L-histidine/Ni^{2+}. CntA and *Sa*NikA are colored gray and cyan, respectively. StP and L-histidine are colored yellow and orange, respectively. The ligand-recognition residues are indicated. (*B*) Structural comparison between the CntA/StP/Co^{2+} complex and the *Bs*NikA/EDTA/Fe^{3+} complex. CntA and *Bs*NikA are colored gray and green, respectively. The ligand-recognition residues are indicated.

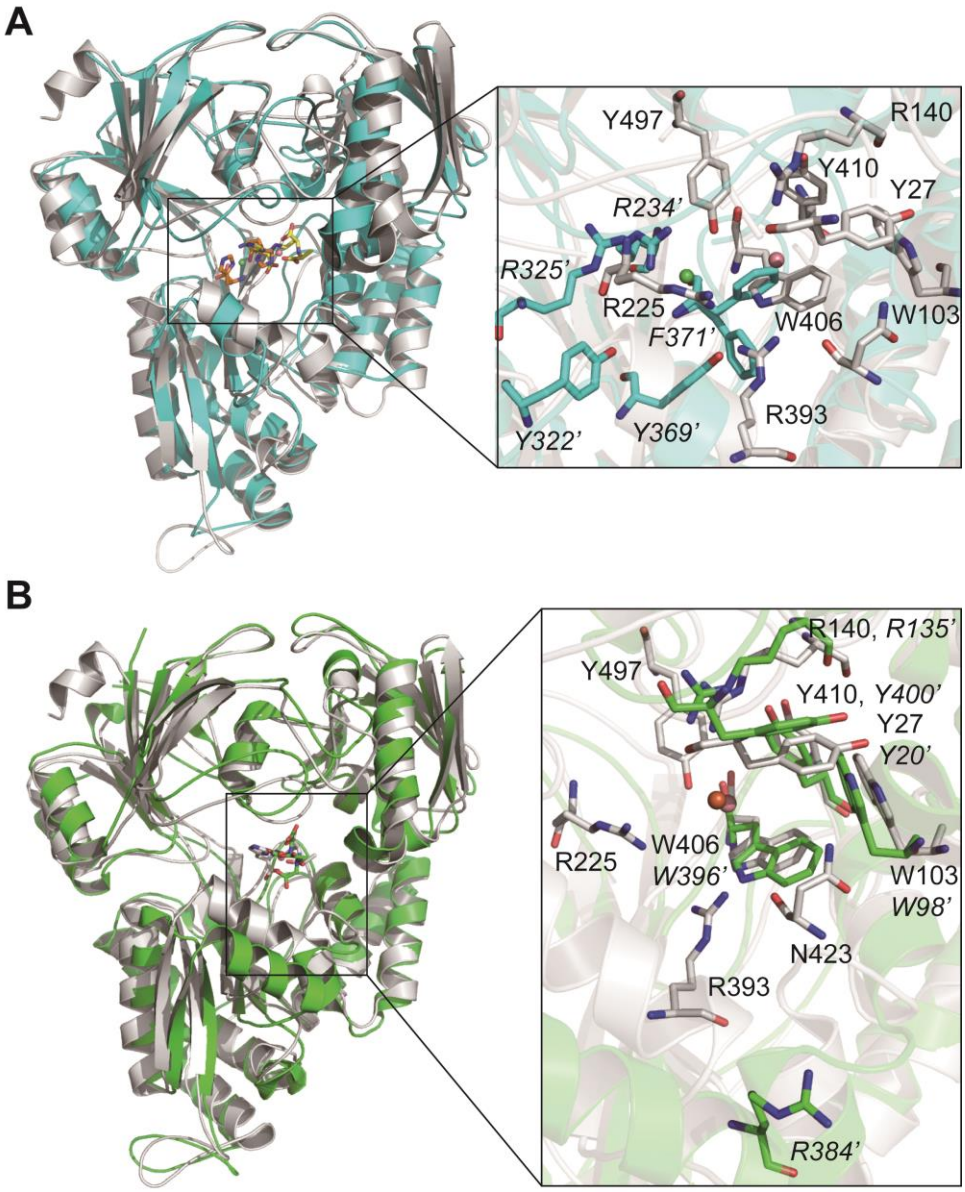

Fig. S14. Single amino-acid mutations of the StP-binding residues do not affect protein expression or stability. (*A*) Size-exclusion chromatography analysis of the wild-type and mutant proteins of CntA. The proteins were analyzed in the HiLoad 16/600 Superdex 200 pg column (GE Healthcare). (*B*) SDS-PAGE analysis of the wild-type and mutant proteins.

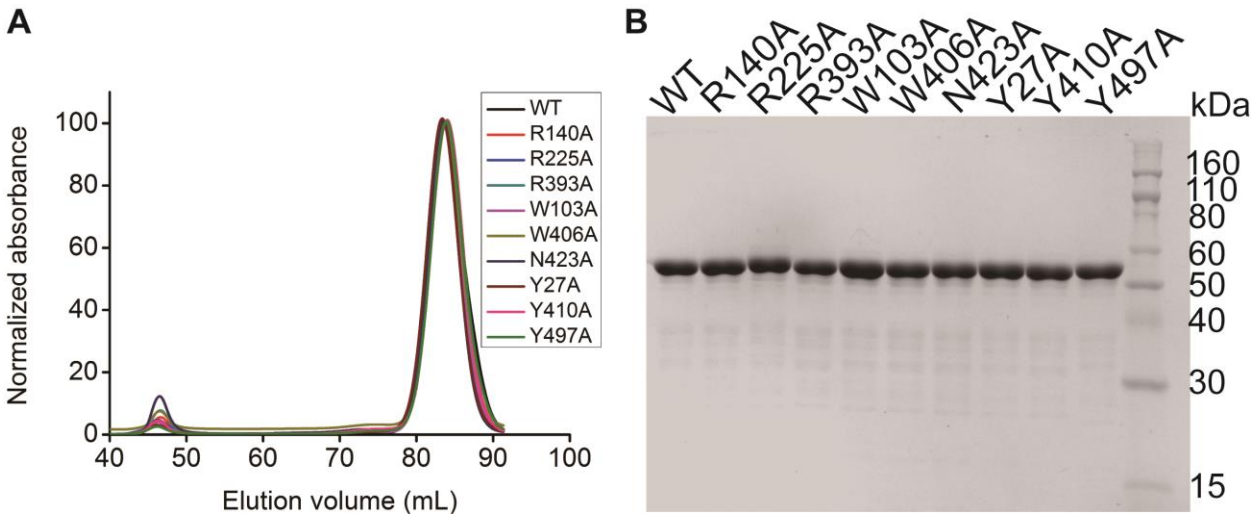

Fig. S15. ITC assays for the binding between StP/Co^{2+} and mutant CntA proteins. K_d: the dissociation constant; N: the number of binding sites per CntA.

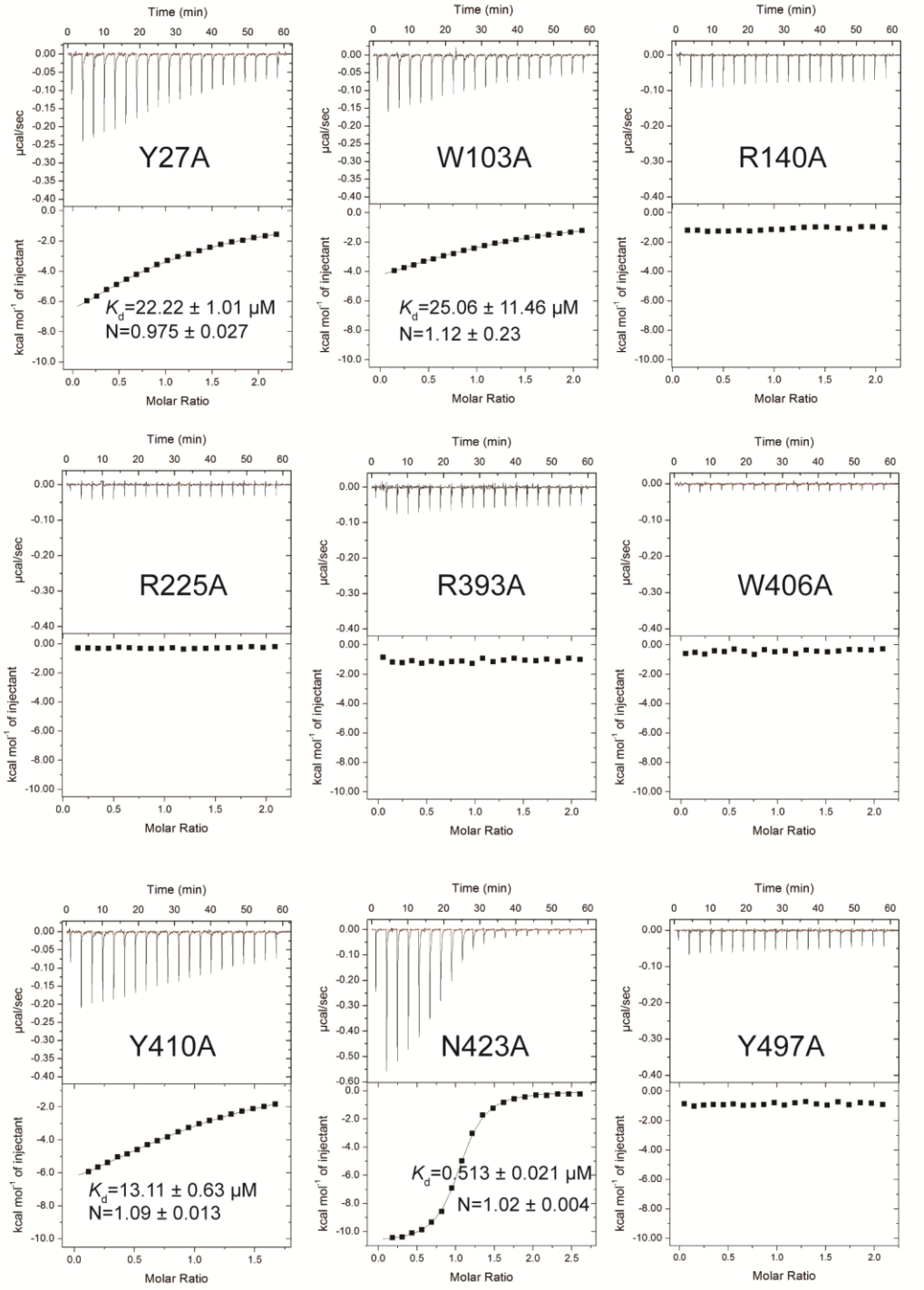

404

Fig. S16. Scheme of the strategy for single-base substitution mutations in the *S. aureus* genome by using the CRISPR/Cas9 system pCasSA. If the desired mutation site is not present in an adjacent protospacer adjacent motif (PAM), a silent mutation will be introduced in the PAM to prevent the cutting of Cas9/sgRNA complex in the genome of edited cells.

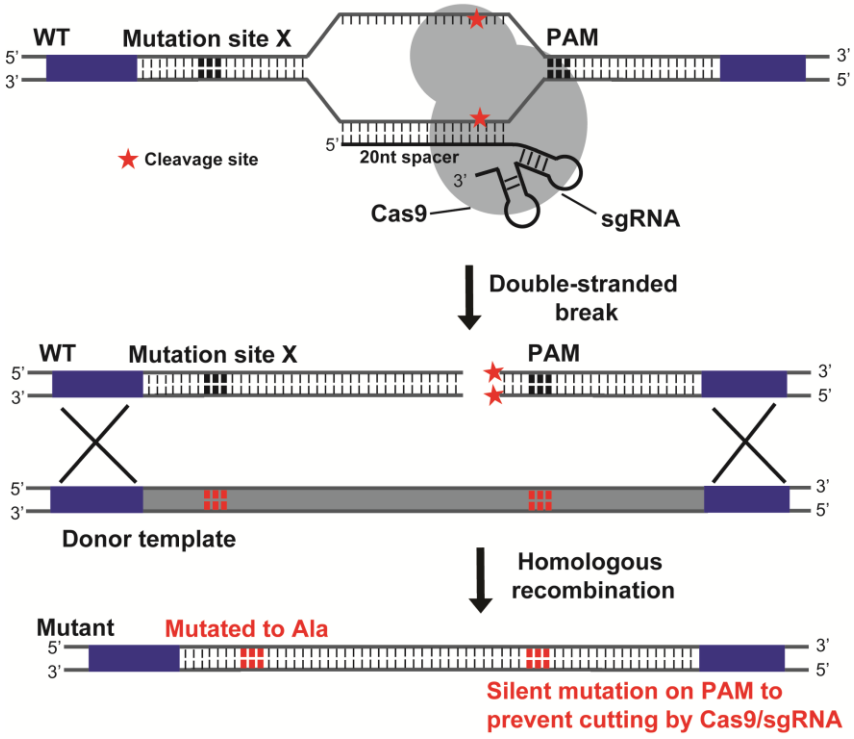

Fig. S17. Growth curve measurements of the Newman mutant and complementation strains in the presence or absence of 1.5 mM Co^{2+}. The assays were performed in the chemically defined medium. Dashed lines: strains were cultured in the absence of 1.5 mM Co^{2+}. Solid lines: strains were cultured in the presence of 1.5 mM Co^{2+}. Dot lines: complementation strains were cultured in the presence of 1.5 mM Co^{2+}.

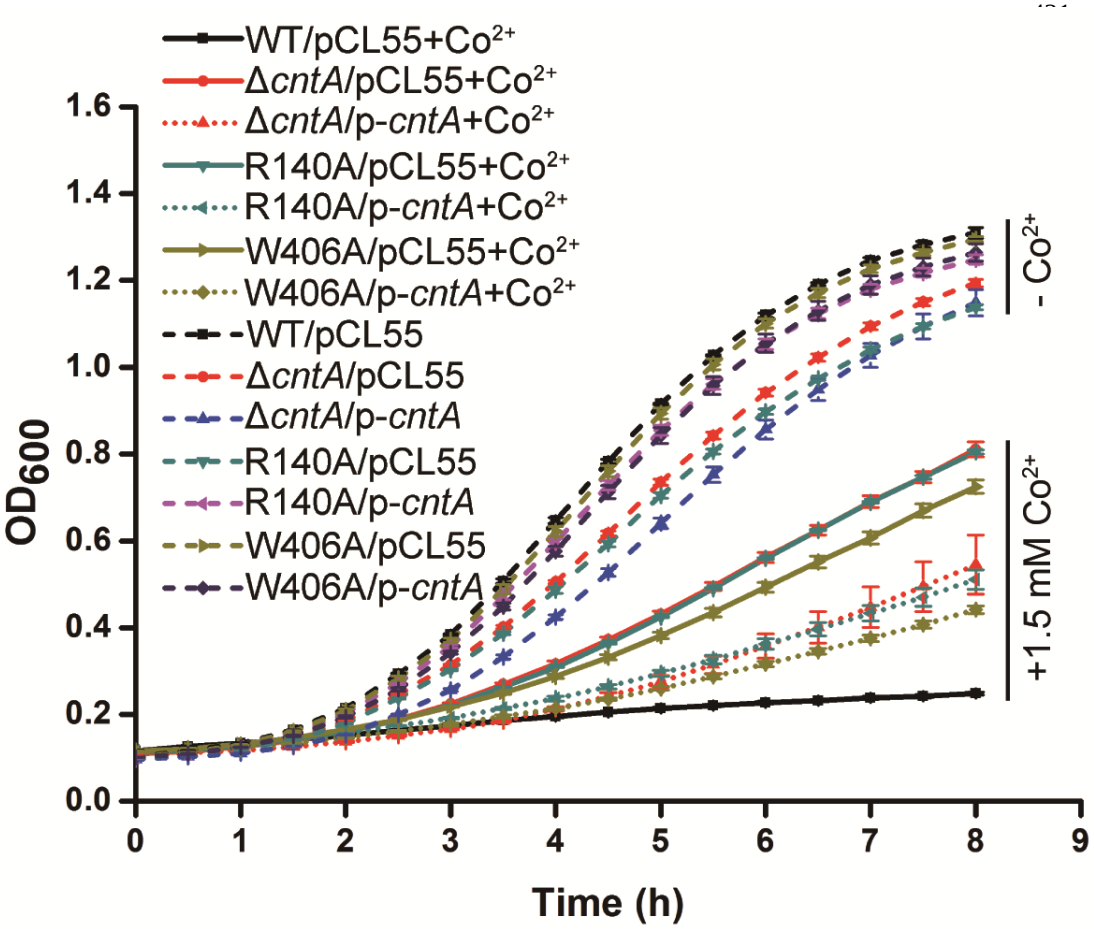

Fig. S18. Co^{2+} accumulation measurements of various strains (Newman) by ICP-AES. (*A*) Co^{2+} accumulation measurements of various mutant strains by ICP-AES. (*B*) Co^{2+} accumulation measurements of various complementation strains by ICP-AES. The assays were performed in CDM the presence of 1 μM Co^{2+}. *: The Co^{2+} amount is below the detection limit of ICP-AES at 7900 atoms/CFU. The *P* values are calculated from Student *t* test.

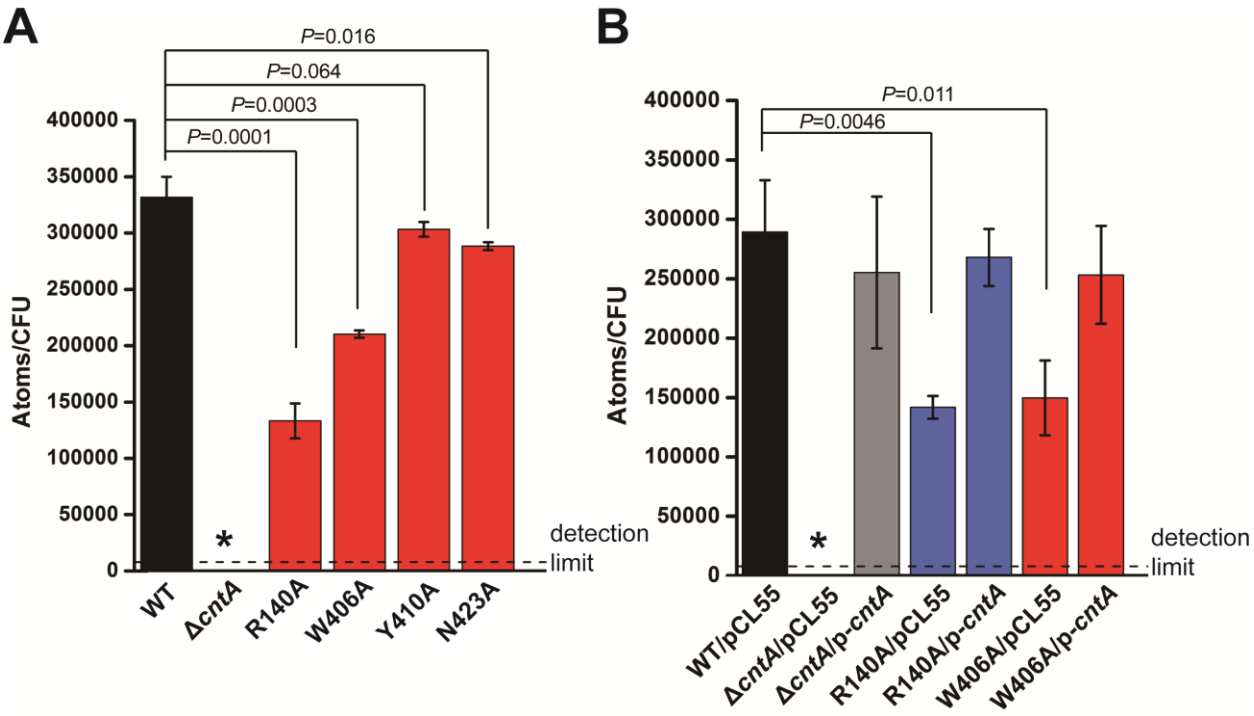

Fig. S19. Sequence alignment of CntA homologous proteins from the StP-like synthesis loci in different bacteria. The StP/metal-recognition residues of CntA are indicated.

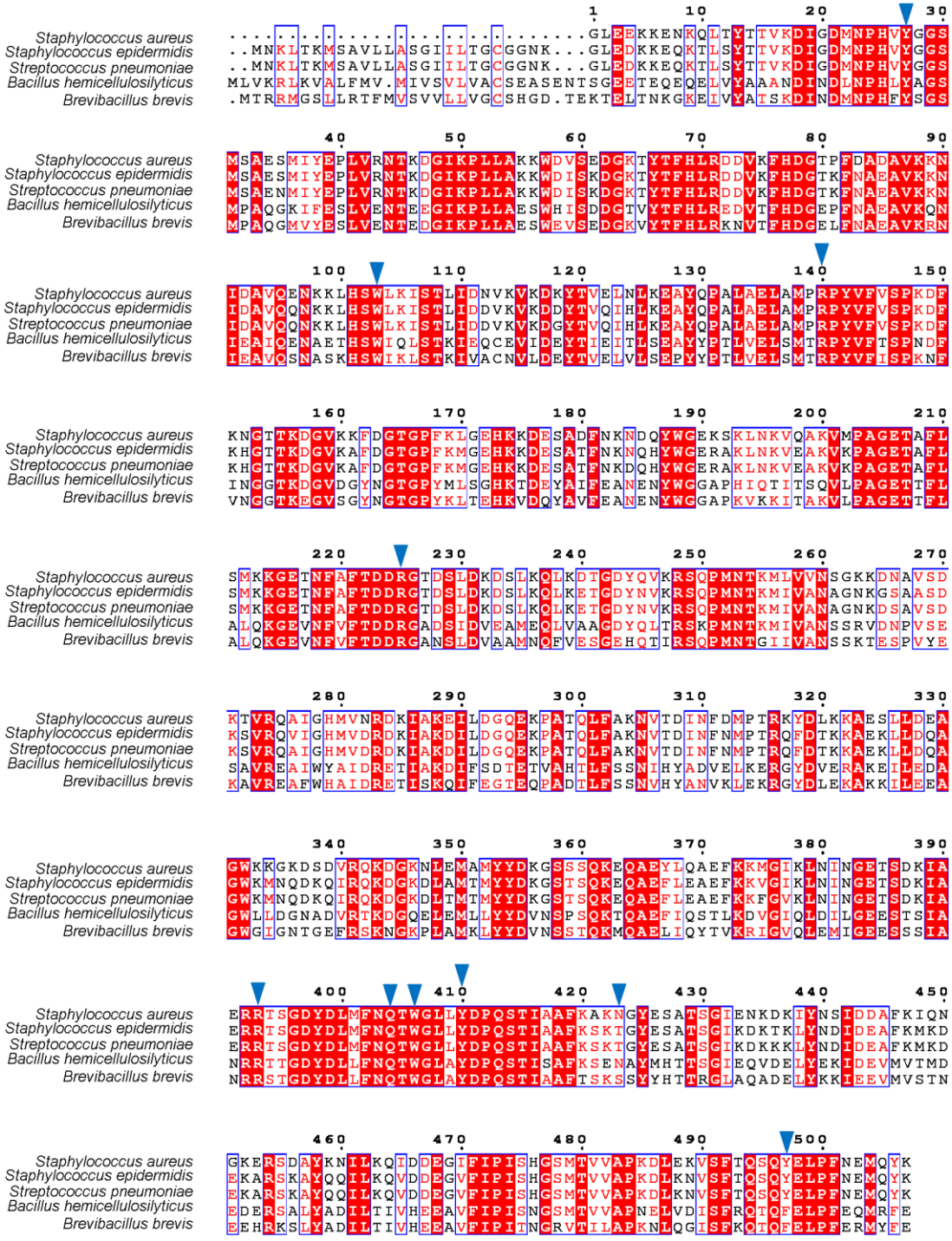

Table S2. Direct and water-mediated interactions between CntA and StP/metal complexes.

		StP/Co^{2+}	StP/Zn^{2+}	StP/Ni^{2+}
Atom of StP	AA interacted	Distance (Å)	Distance (Å)	Distance (Å)
O (1a)	R393	3.1	3.0	3.0
O (1b)	R393	3.0	3.0	2.8
O (1b)	Q404	2.9/2.7*	2.6/2.7*	2.6/2.7*
O (1b)	Y497	2.9/2.7/2.6*	2.6/2.7/2.7*	2.6/2.8/2.5*
O (9b)	N423	3.1	3.1	3.0
N (14)	R225	3.4	3.2	3.4
O (16a)	R140	2.8	2.7	2.8
O (16b)	R140	2.9	3.1	3.1
O (16b)	Y410	2.9/3.0*	2.7/2.6*	2.7/2.7*
C (4)	W406	3.5	3.4	3.3
C (5)	Y410	3.9	3.9	3.9
C (10)	Y497	3.6	3.7	3.7
C (17)	Y27	3.6	3.7	3.8
C (17)	W103	3.4	3.5	3.4
Atom of StP	Distance to Co^{2+} (Å)	Distance to Zn^{2+} (Å)	Distance to Ni^{2+} (Å)	
O (1a)	1.8	2.2	2.0	
N (3)	2.2	2.4	2.3	
N (7)	2.5	2.3	2.1	
O (9a)	1.8	2.0	2.0	
N (12)	2.0	2.0	2.1	
O (16a)	1.9	2.2	2.0	

*Water-mediated hydrogen bonding.

The interactions listed in gray background represent hydrogen bonding. The interactions listed in blue background represent van der Waals interactions. The interactions listed in brown background represent coordination bonding.

Table S3. Strains and plasmids used in this study.

Plasmids or strains	Description	Reference
Plasmids		
pET28a_HRV3C_CntA	pET28a_HRV3C derivative, for expressing CntA, Km^r	This study
pET28a_HRV3C_Y27A	pET28a_HRV3C_CntA derivative, for expressing the CntA_Y27A mutant protein	This study
pET28a_HRV3C_W103A	pET28a_HRV3C_CntA derivative, for expressing the CntA_W103A mutant protein	This study
pET28a_HRV3C_R140A	pET28a_HRV3C_CntA derivative, for expressing the CntA_R140A mutant protein	This study
pET28a_HRV3C_R225A	pET28a_HRV3C_CntA derivative, for expressing the CntA_R225A mutant protein	This study
pET28a_HRV3C_R393A	pET28a_HRV3C_CntA derivative, for expressing the CntA_R393A mutant protein	This study
pET28a_HRV3C_W406A	pET28a_HRV3C_CntA derivative, for expressing the CntA_W406A mutant protein	This study
pET28a_HRV3C_Y410A	pET28a_HRV3C_CntA derivative, for expressing the CntA_Y410A mutant protein	This study
pET28a_HRV3C_N423A	pET28a_HRV3C_CntA derivative, for expressing the CntA_N423A mutant protein	This study
pET28a_HRV3C_Y497A	pET28a_HRV3C_CntA derivative, for expressing the CntA_Y497A mutant protein	This study
pSP_cnt	pSP72 derivative, for the construction of repair templates	This study
pCasSA	*S.aureus* genome editing vector, Km^r, Cm^r	(6)
pCasSA_W103A	pCasSA derivative, for mutation of W103A in *cntA*	This study
pCasSA_R140A	pCasSA derivative, for mutation of R140A in *cntA*	This study
pCasSA_W406A	pCasSA derivative, for mutation of W406A in *cntA*	This study
pCasSA_Y410A	pCasSA derivative, for mutation of Y410A in *cntA*	This study
pCasSA_N423A	pCasSA derivative, for mutation of N423A in *cntA*	This study
pCasSA_*cntA*	pCasSA derivative, for *cntA* deletion	(6)
pCL55	Single-copy integration plasmid, Cm^r, Ap^r	(7)
pCL55_CntA	pCL55 derivative, for *cntA* complementation	This study
Strains		
E.coli		
DH10B	F- *endA*1 *recA*1 *galU galK deoR nupG rpsL* Δ*lacX*74 Φ80*lacZ*ΔM15 *araD*139 Δ(*ara,leu*)7697 *mcrA* Δ(*mrr-hsdRMS-mcrBC*) λ-	Lab stock
ALC7885	*E. coli* K12, Δ*dcm* mutant with pACYC184 containing hsdMS-2^{CC8}, Cm^r	(8)
S. aureus		
RN4220	Restriction-deficient transformation recipient	Lab stock
RN4220_W103A	*cntA* W103A mutation in RN4220	This study
RN4220_R140A	*cntA* R140A mutation in RN4220	This study
RN4220_W406A	*cntA* W406A mutation in RN4220	This study
RN4220_Y410A	*cntA* Y410A mutation in RN4220	This study
RN4220_N423A	*cntA* N423A mutation in RN4220	This study
RN4220_Δ*cntA*	*cntA* gene deletion in RN4220	(6)
Newman	Wild type	(11)
Newman _R140A	*cntA* R140A mutation in Newman	This study
Newman _W406A	*cntA* W406A mutation in Newman	This study
Newman _Y410A	*cntA* Y410A mutation in Newman	This study
Newman _N423A	*cntA* N423A mutation in Newman	This study
Newman _Δ*cntA*	*cntA* gene deletion in Newman	(6)
Newman/pCL55	Newman with empty pCL55	This study
Newman _Δ*cntA*/pCL55	Newman Δ*cntA* mutation with empty pCL55	This study
Newman _Δ*cntA*/p-*cntA*	Newman Δ*cntA* mutation with pCL55_*cntA* complementation	This study
Newman _R140A/pCL55	Newman *cntA* R140A mutation with empty pCL55	This study
Newman _R140A/ p-*cntA*	Newman *cntA* R140A mutation with pCL55_*cntA* complementation	This study
Newman _W406A/pCL55	Newman *cntA* W406A mutation with empty pCL55	This study
Newman _W406A/p-*cntA*	Newman *cntA* W406A mutation with pCL55_*cntA* complementation	This study

Ap^r, ampicillin resistant; Km^r, kanamycin resistant; Cm^r, chloramphenicol resistant.

Table S4. Primers used in this study.

	Name	Sequence (5'-3')	Description
CntA protein	CntA-Fw	cttgaagtcctctttcagggacccCatatgggtttagaggagaaaaaagaaaacaagc	amplification of *cntA* locus from the genomic DNA for expressing the CntA protein
	CntA-Rv	atctcagtggtggtggtggtgctcgagttatttatactgcatttcattgaatggt	
	CntA-Y27A-1	acattgatccaccggcaacatgcggattcatatcaccgatatc	for Y27A mutation in CntA
	CntA-Y27A-2	gatatcggtgatatgaatccgcatgttgccggtggatcaatgt	
	CntA-W103A-1	cattgtcaattaatgtcgaaatctttaacgcagaatgcaatttttgttttcttgaactg	for W103A mutation in CntA
	CntA-W103A-2	cagttcaagaaaacaaaaaattgcattctgcgttaaagatttcgacattaattgacaatg	
	CntA-R140A-1	acacaaatacatatggagcaggcatcgctaattcagccaatg	for R140A mutation in CntA
	CntA-R140A-2	acacaaatacatatggagcaggcatcgctaattcagccaatg	
	CntA-R225A-1	aagctatctgtacctgcatcatctgtgaaggcaaagttcgtttca	for R225A mutation in CntA
	CntA-R225A-2	tgaaacgaactttgccttcacagatgatgcaggtacagatagctt	
	CntA-R393A-1	cattaagtcataatcaccagaagtagcacgttcagcaattttatctgatgtt	for R393A mutation in CntA
	CntA-R393A-2	aacatcagataaaattgctgaacgtgctacttctggtgattatgacttaatg	
	CntA-W406A-1	ggatcgtacaataatcccgcagtttggttgaacattaagtcataatcac	for W406A mutation in CntA
	CntA-W406A-2	gtgattatgacttaatgttcaaccaaactgcgggattattgtacgatcc	
	CntA-Y410A-1	gcaatagtactttgtggatcggccaataatccccaagtttggttg	for Y410A mutation in CntA
	CntA-Y410A-2	caaccaaacttggggattattggccgatccacaaagtactattgc	
	CntA-N423A-1	ttgcactttcataaccagctttcgctttaaatgctgcaatagtactttgtgg	for N423A mutation in CntA
	CntA-N423A-2	ccacaaagtactattgcagcatttaaagcgaaagctggttatgaaagtgcaa	
	CntA-Y497A-1	gaaaaagtatcattcacacaatcacaggctgaattaccattcaatgaaatgcagta	for Y497A mutation in CntA
	CntA-Y497A-2	tactgcatttcattgaatggtaattcagcctgtgattgtgtgaatgatacttttc	
cntA gene deletion	cntA-sp-Fw	GAAAcaagcaaaagtaatgcctgc	spacer for *cntA* gene deletion
	cntA-sp-Rv	AAACgcaggcattacttttgcttg	
	cntA-UpFw	TTTGAGATCTGTCCATACCCATGGTCTAGAacatgggatcgacacattca	amplification of ~1kb *cntA* upstream for gene deletion
	cntA-UpRv	ttctcaatgcctgatgttgcTTGCTTTTCCTCTTTCTAAATTGATAAGTTG	
	cntA-DnFw	CAACTTATCAATTTAGAAAGAGGAAAAGCAAgcaacatcaggcattgagaa	amplification of ~1kb *cntA* downstream for gene deletion
	cntA-DnRv	AAGATACAGGTATATTTTTCTGACTCGAGctagtccaggccatgcaaag	
	cntAsqFw	GCCAGGCGTACAAGGATATG	sequencing of *cntA* locus
cntA gene complementation	CntA-pCL1	cctttcgtcttcaagaattctaagggtttgaagttttataatagaaaaa	amplification of *cnt* operon promoter from the genomic DNA
	CntA-pCL2	atatgctttaattcacttcattatttatactgcatttcattgaatgg	
	CntA-pCL3	cattcaatgaaatgcagtataaataatgaagtgaattaaagcatattaagttaa	amplification of *cntA* gene from the genomic DNA
	CntA-pCL4	ttttacatccctccGGATCCagaatgtttcatgtcctagca	
cntA gene mutation	cnt1	attcgagctcggtacccggggatccTCTAGAaagtcgttgaatcgccactg	amplification of ~4kb *cntA* gene and up and down regions for

	cnt2	atacgatttaggtgacactatagaaCTCGAGatgtcacaagtgg tgctgct	gene mutation
W103A	CntA-F68F-1	ttaacgtcatctctcaaatgaaacgtgtatgtcttcccatc	for *cntA*_F68F silent mutation
	CntA-F68F-2	gatgggaagacatacacgtttcatttgagagatgacgttaa	
	F68-sp-Fw	GAAAatttaacgtcatctctcaaa	spacer for *cntA*_W103A mutation
	F68-sp-Rv	AAACtttgagagatgacgttaaat	
	W103A-UpFw	TTTGAGATCTGTCCATACCCATGGTCTAG Aaggaccgataacgatgacacta	amplification of ~2 kb repair for *cntA*_W103A mutation
	W103A-DnRv	AAGATACAGGTATATTTTTCTGACTCGAGa gtttggttgaacattaagtcataatc	
R140A	CntA-F209F-1	cgtttcacctttttcattgataaaaatgctgtttcaccagcaggcatt	for *cntA*_F209F silent mutation
	CntA-F209F-2	aatgcctgctggtgaaacagcatttttatcaatgaaaaaaggtgaaac g	
	F209-sp-Fw	GAAAtttcacctttttcattgat	spacer for *cntA*_R140A mutation
	F209-sp-Rv	AAACatcaatgaaaaaaggtgaaa	
	R140A-UpFw	TTTGAGATCTGTCCATACCCATGGTCTAG Aaggaccgataacgatgacacta	amplification of ~2 kb repair for *cntA*_R140A mutation
	R140A-DnRv	AAGATACAGGTATATTTTTCTGACTCGAGa gtttggttgaacattaagtcataatc	
W406A	W406-sp-Fw	GAAAacttaatgttcaaccaaact	spacer for *cntA*_W406A mutation
	W406-sp-Rv	AAACagtttggttgaacattaagt	
	W406A-UpFw	TTTGAGATCTGTCCATACCCATGGTCTAG A gcggtggatcaatgtctgctg	amplification of ~2 kb repair for *cntA*_W406A mutation
	W406A-DnRv	AAGATACAGGTATATTTTTCTGACTCGAG atgtcacaagtggtgctgct	
Y410A	CntA-I448I-1	caacagcattgatgacgcatttaaaatacaaaacggtaaagagc	for *cntA*_I448I silent mutation
	CntA-I448I-2	gctctttaccgttttgtattttaaatgcgtcatcaatgctgttg	
	I448-sp-Fw	GAAActgaacgctctttaccgttt	spacer for *cntA*_Y410A, N423A mutation
	I448-sp-Rv	AAACaaacggtaaagagcgttcag	
	Y410A-UpFw	TTTGAGATCTGTCCATACCCATGGTCTAG A cggtggatcaatgtctgctg	amplification of ~2 kb repair for *cntA*_Y410A, N423A mutation
	Y410A-DnRv	AAGATACAGGTATATTTTTCTGACTCGAG atgtcacaagtggtgctgct	

REFERENCES

1. Minor W, Cymborowski M, Otwinowski Z, & Chruszcz M (2006) HKL-3000: the integration of data reduction and structure solution--from diffraction images to an initial model in minutes. *Acta Crystallogr D Biol Crystallogr* 62(Pt 8):859-866.
2. Read RJ (2001) Pushing the boundaries of molecular replacement with maximum likelihood. *Acta Crystallogr D Biol Crystallogr* 57(Pt 10):1373-1382.
3. Collaborative Computational Project N (1994) The CCP4 suite: programs for protein crystallography. *Acta Crystallogr D Biol Crystallogr* 50(Pt 5):760-763.
4. Adams PD, *et al.* (2010) PHENIX: a comprehensive Python-based system for macromolecular structure solution. *Acta Crystallogr D Biol Crystallogr* 66(Pt 2):213-221.
5. Emsley P & Cowtan K (2004) Coot: model-building tools for molecular graphics. *Acta Crystallogr D Biol Crystallogr* 60(Pt 12 Pt 1):2126-2132.
6. Chen W, Zhang Y, Yeo WS, Bae T, & Ji Q (2017) Rapid and Efficient Genome Editing in *Staphylococcus aureus* by Using an Engineered CRISPR/Cas9 System. *J Am Chem Soc* 139(10):3790-3795.
7. Lee CY, Buranen SL, & Ye ZH (1991) Construction of single-copy integration vectors for *Staphylococcus aureus*. *Gene* 103(1):101-105.
8. Jones MJ, Donegan NP, Mikheyeva IV, & Cheung AL (2015) Improving transformation of *Staphylococcus aureus* belonging to the CC1, CC5 and CC8 clonal complexes. *PLoS One* 10(3):e0119487.
9. Remy L, *et al.* (2013) The *Staphylococcus aureus* Opp1 ABC transporter imports nickel and cobalt in zinc-depleted conditions and contributes to virulence. *Mol Microbiol* 87(4):730-743.
10. Ghssein G, *et al.* (2016) Biosynthesis of a broad-spectrum nicotianamine-like metallophore in *Staphylococcus aureus*. *Science* 352(6289):1105-1109.
11. Duthie ES, Lorenz LL (1952) Staphylococcal coagulase: mode of action and antigenicity. *J Gen Microbiol* 6:95–107.